

Data-driven discovery of Bäcklund transforms and soliton evolution equations via deep neural network learning schemes

Zijian Zhou^{1,2}, Li Wang^{3,4}, and Zhenya Yan^{1,2,*}

¹*Key Laboratory of Mathematics Mechanization, Academy of Mathematics and Systems Science,
Chinese Academy of Sciences, Beijing 100190, China*

²*School of Mathematical Sciences, University of Chinese Academy of Sciences, Beijing 100049, China*

³*Yanqi Lake Beijing Institute of Mathematical Sciences and Applications, Beijing, 101408, China*

⁴*Yau Mathematical Sciences Center and Department of Mathematics, Tsinghua University, Beijing, 100084, China*

Abstract. We introduce a deep neural network learning scheme to learn the Bäcklund transforms (BTs) of soliton evolution equations and an enhanced deep learning scheme for data-driven soliton equation discovery based on the known BTs, respectively. The first scheme takes advantage of some solution (or soliton equation) information to study the data-driven BT of sine-Gordon equation, and complex and real Miura transforms between the defocusing (focusing) mKdV equation and KdV equation, as well as the data-driven mKdV equation discovery via the Miura transforms. The second deep learning scheme uses the explicit/implicit BTs generating the higher-order solitons to train the data-driven discovery of mKdV and sine-Gordon equations, in which the high-order solution informations are more powerful for the enhanced learning soliton equations with higher accuracies.

Keywords: Deep neural networks; Bäcklund transform; Miura transform; soliton evolution equations; breathers

1 Introduction

In the fields of applied mathematics and nonlinear mathematical physics, there are many types of physically interesting nonlinear evolution partial differential equations (PDEs). Particularly, since the well-known Korteweg-de Vries (KdV) equation with solitons (or solitary waves) [1, 2] was presented by Korteweg and de Vries [3], various of soliton evolution equations [4, 5] (e.g., Boussinesq equation, mKdV equation, KP equation, sine-Gordon equation, nonlinear Schrödinger equation, Gross-Pitaevskii equation) play an important role in the fields of nonlinear science such as fluid mechanics, nonlinear optics, quantum optics, Bose-Einstein condensates, plasmas physics, ocean, atmosphere, biology, and even finance [6–11]. Many types of analytical, numerical and experimental approaches have been used to deeply explore the wave structures and properties of these soliton equations (see, e.g., Refs. [4–12] and references therein).

Since Bäcklund [13] first found a transform (alias the auto-Bäcklund transform (aBT)) of the sine-Gordon equation $u_{xt} = \sin u$ in 1875, and Darboux [14] found a transform (alias Darboux transform) of the Sturm-Liouville equation (alias the linear Schrödinger equation) $\psi_{xx} + [\lambda - V(x)]\psi = 0$ in 1882, many types of well-known analytical transforms were found between the same equation or different equations [15–23]. For example, Hopf [24] and Cole [25] independently established a BT between the nonlinear Burgers equation $u_t + uu_x - \mu u_{xx}$ and linear heat (or diffusion) equation $v_t - \mu v_{xx} = 0$ in 1950–1951. In 1967, Gardner, Greene, Kruskal, and Miura (GGKM) [26] solved the initial value problem of the KdV equation starting from its coupled linear PDEs, which are just its Lax pair [5]. In 1968, strongly motivated by the GGKM’s idea, Lax [27] presented a general formal BT (alias Lax pair) implying that the eigenvalues of the linear operator $\{L(\phi)\psi = \lambda\psi(\phi), \psi_t = B(\phi)\psi\}$ are integrals of the nonlinear equation $\phi_t = K(\phi)$. In the same year, Miura [28] found a new BT (alias Miura transform) between the KdV equation $v_t + 6vv_x + v_{xxx} = 0$ and focusing (or defocusing) mKdV equation $u_t \pm 6u^2u_x + u_{xxx} = 0$.

* *Email address:* zyyan@mmrc.iss.ac.cn (Corresponding author)

With the quick development of cloud computing resources and mass data, deep learning [29,30] has been used in many fields containing cognitive science [31], image recognition [32], genomics [33], industrial areas [34,35], and etc. In particular, in the past of decades, some deep neural network learning methods [36–44] have been developed to study the partial differential equations (PDEs), which play an important role in the various of scientific fields. The powerful physics-informed neural network (PINN) method [43,44] was used to investigate the PDEs [45–51], the fractional PDEs [52], and stochastic PDEs [53].

In this paper, we would like to develop two kinds of deep neural network learning methods to study the discovery of BTs and soliton equations via the general system

$$\begin{cases} F(u, u_t, u_x, u_{tt}, u_{tx}, u_{xx}, \dots) = 0, & (1a) \\ G(u', u'_t, u'_x, u'_{tt}, u'_{tx}, u'_{xx}, \dots) = 0, & (1b) \\ \phi_i(u, u_t, u_x, u_{tt}, u_{tx}, u_{xx}, \dots, u', u'_t, u'_x, u'_{tt}, u'_{tx}, u'_{xx}, \dots) = 0, \quad (i = 1, 2, \dots), & (1c) \end{cases}$$

where $u = u(x, t)$, $u' = u'(x, t)$, the considered spatio-temporal region is $(x, t) \in [-L, L] \times [-T, T]$, Eq. (1c) is called the BT between Eqs. (1a) and (1b). In particular, if Eq. (1b) is equivalent to Eq. (1a), then the transform (1c) is called the aBT. It is obvious to see that the information of Eq. (1a) can be shifted to Eq. (1b) with the aid of BT (1c). Sometimes, the structures of the transformed Eq. (1b) may become more simpler. Therefore, BTs can be used to discover the new information of Eqs. (1a) and (1b).

The rest of the paper is organized as follows. In Sec. 2, we will introduce a deep neural network learning scheme to study aBTs and BTs, e.g., the aBT of the sine-Gordon equation, and Miura transform between the focusing/defocusing mKdV equation and KdV equation. Moreover, the deep learning scheme can also be used to discover soliton equations with the aid of BTs. In Sec. 3, a new deep learning method for soliton equation discovery is displayed based on BTs. We use the implicit and explicit BTs to exhibit the data-driven discovery of sine-Gordon equation and mKdV equation with the aid of aBT of the sine-Gordon equation, and Darboux transform of the focusing mKdV equation, respectively. Finally, some conclusions and discussions are presented in Sec. 4.

2 Data-driven discovery of BTs and soliton equations

2.1 Deep learning scheme for the BT discovery

We here would like to introduce the deep learning scheme for the discovery of BTs and soliton equations by examining system (1). The main idea of this scheme is to use some constraints on $u(x, t)$ and $u'(x, t)$ to find the approximate transform between $u(x, t)$ and $u'(x, t)$, where $u(x, t)$ and $u'(x, t)$ are represented by one or two deep neural networks. There are many kinds of neural networks including the fully-connected neural network, convolution neural network, and recurrent neural network. The constraints of the functions include the real solution data-set and the corresponding equations. The aim of the scheme is to make the neural network solution approach to the real data better and match some physical laws efficiently.

Figure 1 displays the deep learning scheme of the BT discovery, where $u(x, t)$ and $u'(x, t)$ are represented by a deep neural network, which is, in general, chosen as a fully-connected neural network. It will share the network parameters, weights, and biases. For some conditions, they can be represented by two different networks to eliminate mutual influence. In this diagram, we assume that $u(x, t)$ and $u'(x, t)$ are real-valued functions. If the solutions of Eq. (1a) are complex, the number of output neurons would be double. The number of input neurons equals to the independent variables of $u(x, t)$ and $u'(x, t)$. τ represents the activation function, and is chosen as $\tau(x) = \tanh(x)$ in this scheme, whose aim is to add the nonlinear action to the deep neural network. Notice that one can also choose other types of activation functions such as the sigmoid (logistic) function, threshold function, piecewise linear function, ReLU function, ELU function, swish function, and softmax function.

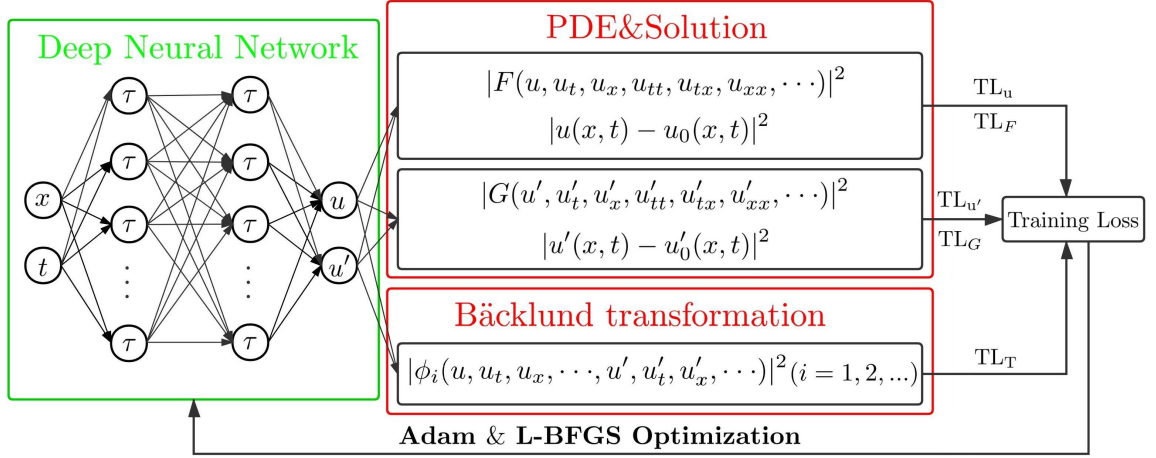


Figure 1: The deep learning scheme for the data-driven discovery of BTs and soliton equations.

The loss function during the training process consists of two different parts. It can be simply written as:

$$TL = TL_T + TL_{F/u} + TL_{G/u'}. \quad (2)$$

with

$$\begin{aligned} TL_F &= \frac{1}{N_p} \sum_{j=1}^{N_p} |F(u(x_j, t_j), u_t(x_j, t_j), u_x(x_j, t_j), \dots)|^2, \\ TL_u &= \frac{1}{N_p} \sum_{j=1}^{N_p} |u(x_j, t_j) - u_0(x_j, t_j)|^2, \\ TL_G &= \frac{1}{N_p} \sum_{j=1}^{N_p} |G(u'(x_j, t_j), u'_t(x_j, t_j), u'_x(x_j, t_j), \dots)|^2, \\ TL_{u'} &= \frac{1}{N_p} \sum_{j=1}^{N_p} |u'(x_j, t_j) - u'_0(x_j, t_j)|^2, \\ TL_T &= \frac{1}{N_p} \sum_{j=1}^{N_p} |\phi_j(u, u_t, u_x, \dots, u', u'_t, u'_x, \dots)|^2_{(x,t)=(x_j, t_j)}, \end{aligned} \quad (3)$$

where $\{x_j, t_j\}_{j=1}^{N_p}$ denote the set of sampling points in some spatio-temporal region $(x, t) \in [-L, L] \times [-T, T]$, N_p stands for the number of sampling points, which are generated by using the Latin Hypercube Sampling strategy [54], and $u_0(x, t)$ and $u'_0(x, t)$ represent the sampling solution data of Eqs. (1a) and (1b), respectively.

We would like to use the above-mentioned framework to study two tasks. In the first task, we aim to learn the unknown BTs. $\phi_j(\cdot)$'s in the training loss TL_T contain all the possible terms under the principle of homogeneity. And the constraints arising from the loss functions TL_u (or TL_F) and $TL_{u'}$ (or TL_G) will make ϕ_j 's approach to the exact BT. Moreover the correct parameters will be found. For the second task, we assume that the G in Eq. (1b) is unknown. If $u'(x, t)$ can be explicitly represented by $u(x, t)$, then the data-set of $u(x, t)$ can be converted to the data-set of $u'(x, t)$. Thus we assume that $u'(x, t)$ is implicit about $u(x, t)$. We assume that G has some possible terms under the principle of homogeneity. The equation can be discovered when the constraints produced by TL_u , TL_G and TL_T . We can learn G only using the data-set of F .

In the scheme, firstly, for a set of larger sampling points, we would like to use an efficient mini-batch optimization algorithm Adam [55]. Secondly, the model will be trained by a full-batch optimization algorithm L-BFGS [56] until the difference of the loss function is less than the Machine Epsilon. In what follows, we will use some examples to verify the validity of our deep learning scheme.

2.1.1 Data-driven BT discovery of the sine-Gordon equation

The well-known sine-Gordon (s-G) equation [57]

$$u_{xt} = \sin u, \quad u(x, t) \in \mathbb{R}[x, t] \quad (4)$$

is a physical interesting model, and can be used to describe the theory of crystal dislocations, Bloch-wall motion, splay waves in lipid membranes, magnetic flux on a Josephson line, and elementary particles [58–60]. The s-G equation (4) admits the auto-Bäcklund transform (aBT) [13]

$$\begin{cases} u'_x = u_x - 2\beta \sin\left(\frac{u+u'}{2}\right), \\ u'_t = -u_t + \frac{2}{\beta} \sin\left(\frac{u-u'}{2}\right), \end{cases} \quad (5)$$

where $\beta \neq 0$ is an arbitrary real-valued constant, that is, if $u(x, t)$ is a solution of the s-G equation (4), then so is $u'(x, t)$ given by Eq. (5). In what follows, we would like to use the above-mentioned deep learning method to discover the parameters of the aBT (5). For convenience, we consider the generalized aBT

$$\begin{cases} u'_x = au_x - b \sin\left(\frac{u+u'}{2}\right) + hu_x, \\ u'_t = -cu_t + d \sin\left(\frac{u-u'}{2}\right) - fu_t. \end{cases} \quad (6)$$

where the parameters a, b, c, d, h , and f are real-valued parameters to be determined later, the two new quadratic nonlinear terms are introduced in the unknown aBT (6). In particular, as $a = c = 1, b = 2\beta, d = 2/\beta, h = f = 0$, the unknown aBT (6) reduces to the known exact aBT (5).

We use the above-mentioned deep leaning scheme to discover the aBT of the s-G equation in two cases by considering the system

$$\begin{cases} u'_{xt} - \sin u' = 0, \\ u'_x - au_x + b \sin\left(\frac{u+u'}{2}\right) - hu_x = 0, \\ u'_t + cu_t - d \sin\left(\frac{u-u'}{2}\right) + fu_t = 0. \end{cases} \quad (7)$$

in the spatio-temporal region $(x, t) \in [-10, 10] \times [-5, 5]$, where a, b, c, d, h , and f are parameters to be determined. The training data are generated by following the breather solution of the s-G equation (4) [59]

$$u = 4 \arctan\left(\frac{\tan(\mu)\sin(X \cos(\mu))}{\cosh(T \sin(\mu))}\right), \quad X = \frac{(1-k)x - (1+k)t}{\sqrt{1-k^2}}, \quad T = \frac{(1-k)x + (1+k)t - x_0}{\sqrt{1-k^2}}, \quad (8)$$

where $k \in [0, 1), \mu \neq 0$.

Here, the hidden neural network $\hat{u}(x, t)$ in Python can be defined as

```

def u(x, t):
    U = neural_net(tf.concat([x,t],1), weights, biases)
    u = U[:, 0:1]
    v = U[:, 1:2]
    return u, v

```

such that the residual neural network $f_{sG}(x, t)$ and $f_{BT}(x, t)$ in Python can be obtained as

```

def f_sG(x, t):
    u, v = u(x, t)
    v_t = tf.gradients(v, t)[0]
    v_x = tf.gradients(v, x)[0]
    v_xt = tf.gradients(v_x, t)[0]
    u_x = tf.gradients(u, x)[0]
    u_t = tf.gradients(u, t)[0]
    f_sG = v_xt - sin(v)
    f_BT1 = v_x - a * u_x + b * tf.sin((u + v) / 2) - h * u * u_x
    f_BT2 = v_t + c * u_t - d * tf.sin((u - v) / 2) + f * u * u_t
    return f_sG, f_BT1, f_BT2

```

Case A.—In this case, we suppose that a, b, c , and d are unknown parameters, and $h = f = 0$. It should be pointed out that the two parameters b and d are not fixed. We know that $bd = 4$ in the given exact aBT (5) such that we only consider the product value of b and d in the deep learning. We use a 6-layer neural network with 5 hidden layers and 40 neurons per layer to learn system (7). Without loss of generality, we take the initial value of all free parameters as 1, i.e., $a = b = c = d = 1$. We choose $(x, t) \in [-10, 10] \times [-5, 5]$ as the training region, from which 10,000 sample points are taken by Latin Hypercube Sampling strategy [54]. Moreover, the 20,000 steps Adam and 50,000 steps L-BFGS optimizations are used in the deep learning. Fig. 2(a) displays the trained breather solution by using the deep neural network. Case A in Table 1 exhibits the learning parameters about a, c, b and d , and their errors under two senses of the training data without a noise and with a 2% noise, which imply that the used deep learning method is effective. Moreover, the errors are exhibited in Figs. 2(b1, b2) for the cases without a noise and with a 2% noise, respectively. The training times are 619.92s and 637.08s, respectively.

Case B.—In this case, we suppose that a, b, c, d, h , and f are all unknown parameters. We used the same deep neural network method as Case A to study this case. Case B in Table 1 displays the learning parameters about a, b, c, d, h , and f , and their errors under two senses of the training data without a noise and with a 2% noise, which imply that the used deep learning method is effective. Moreover, the errors are exhibited in Figs. 2(b3, b4) for the cases without a noise and with a 2% noise, respectively. The training times are 659.96s and 697.76s, respectively.

2.1.2 Data-driven discovery of Miura transforms

In 1968, Miura [28] presented the well-known complex Miura transform (a special BT)

$$v = iu_x + u^2, \quad i = \sqrt{-1}, \quad (9)$$

and real Miura transform

$$v = u_x - u^2 \quad (10)$$

to transform, respectively, the focusing mKdV equation [5, 28]

$$u_t + 6u^2u_x + u_{xxx} = 0 \quad (11)$$

Table 1: Data-driven discovery of parameters a, bd, c, h, f in aBT (6) and errors, as well as training times.

Case	a	$b \cdot d$	c	h	f	
Exact	1	4	1	0	0	
A (no noise)	1.00007	4.00006	1.00001	0	0	
A (2% noise)	0.99995	4.00057	1.00003	0	0	
B (no noise)	1.00004	4.00021	1.00001	-4.24×10^{-7}	-2.51×10^{-6}	
B (2% noise)	0.99988	3.99959	0.99985	-3.90×10^{-4}	-3.60×10^{-4}	
Case	error of a	error of $b \cdot d$	error of c	error of h	error of f	time
A (no noise)	7.44×10^{-5}	6.45×10^{-5}	1.31×10^{-5}	0	0	619.92s
A (2% noise)	5.29×10^{-4}	5.74×10^{-4}	3.24×10^{-5}	0	0	637.08s
B (no noise)	4.17×10^{-5}	2.12×10^{-4}	1.37×10^{-5}	4.24×10^{-7}	2.51×10^{-6}	659.96s
B (2% noise)	1.20×10^{-4}	4.05×10^{-4}	1.47×10^{-4}	3.94×10^{-4}	3.57×10^{-4}	697.76s

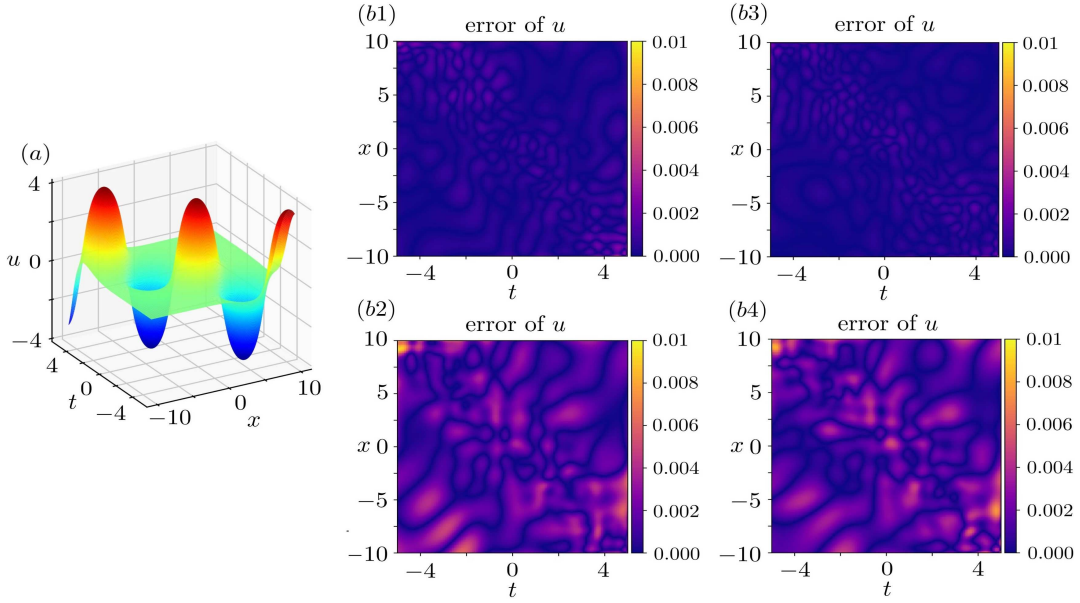


Figure 2: Data-driven aBT discovery of the sine-Gordon equation (4): (a) breather solution (8) generating the training data; (b1-b4) Relative error between exact solution and neural network solution: (b1, b3) training data without a noise; (b2, b4) training data with a 2% noise. The relative \mathbb{L}^2 -norm errors of $u(x, t)$, respectively, are (b1) $3.5255 \cdot 10^{-4}$, (b2) $1.3327 \cdot 10^{-3}$, (b3) $2.7313 \cdot 10^{-4}$, and (b4) $1.3390 \cdot 10^{-3}$. Training times in (b1-b4) are 619.92s, 659.96s, 637.08s, and 697.76s, respectively.

and the defocusing mKdV equation [5, 28]

$$u_t - 6u^2u_x + u_{xxx} = 0 \quad (12)$$

Table 2: Data-driven discovery of the complex Miura transform (14) via system (15): a , b , c , d and their errors, as well as the training times.

Case	a	b	c	d	
Exact	1	1	0	0	
A (no noise)	0.99931	0.99958	0	0	
A (2% noise)	1.00026	0.99981	0	0	
B (no noise)	1.00006	0.99990	-4.1×10^{-4}	-1.0×10^{-5}	
B (2% noise)	1.00017	0.99994	-1.3×10^{-4}	2.0×10^{-4}	
Case	error of a	error of b	error of c	error of d	time
A (no noise)	6.94×10^{-4}	4.25×10^{-4}	0	0	609.30s
A (2% noise)	2.58×10^{-4}	1.89×10^{-4}	0	0	645.68s
B (no noise)	6.00×10^{-5}	1.03×10^{-4}	4.05×10^{-4}	5.00×10^{-6}	635.56s
B (2% noise)	1.68×10^{-4}	5.90×10^{-5}	1.32×10^{-4}	1.99×10^{-5}	637.18s

into the same KdV equation [3]

$$v_t + 6vv_x + v_{xxx} = 0, \quad (13)$$

which can describe the shallow water wave, pressure waves, acoustic waves, magneto-sonic waves, electron plasma waves, and ion acoustic waves [61, 62].

In this subsection, the data-driven deep learning method will be used in two different cases. In the first part, the parameters of Miura transform will be discovered including with and without disturbance terms. The data-set is generated by an exact soliton solution of mKdV and an corresponding exact solution of KdV equation, which is generated by following soliton solution through Miura transform. In the second part, an equation will be discovered through the solution of another equation. The data-set is generated by the solution of another equation. The real Miura transform will be used in the loss function to find the unknown equation.

Case 1. Data-driven discovery of complex Miura transform

In the following, we would like to study the data-driven parameter discovery of the complex Miura transform. We consider the generalized Miura transform

$$v = iau_x + bu^2 + cuu_x + du_{xx}. \quad (14)$$

where a, b, c, d are four parameters to be determined. If $a = b = 1, c = d = 0$, then the transform (14) reduces to the known Miura transform.

In the following, we would like to use the above-mentioned deep leaning scheme to discovery these parameters a, b, c, d of the complex Miura transform (14) between the focusing mKdV equation and KdV equation in two cases by considering the system

$$\begin{cases} u_t + 6u^2u_x + u_{xxx} = 0, \\ v_t + 6vv_x + v_{xxx} = 0, \\ v - iau_x - bu^2 - cuu_x - du_{xx} = 0. \end{cases} \quad (15)$$

Table 3: Data-driven discovery of real Miura transform (18) via system (19): a , b , c , d and their errors, as well as the training times.

Case	a	b	c	d	
Exact	1	-1	0	0	
Case A (no noise)	0.99999	-1.00000	0	0	
Case A (2% noise)	1.00026	-1.00012	0	0	
Case B (no noise)	1.00000	-0.99999	0.00011	-0.00013	
Case B (2% noise)	1.00019	-1.00023	0.00271	-0.00303	

Case	error of a	error of b	error of c	error of d	time
Case A (no noise)	1.36×10^{-5}	1.35×10^{-6}	0	0	374.40s
Case A (2% noise)	2.55×10^{-4}	1.22×10^{-4}	0	0	407.44s
Case B (no noise)	7.39×10^{-6}	5.66×10^{-6}	1.14×10^{-4}	1.25×10^{-4}	405.32s
Case B (2% noise)	1.85×10^{-4}	2.31×10^{-5}	2.71×10^{-3}	3.03×10^{-3}	417.00s

The training data-set is generated by the bright soliton of the focusing mKdV equation (11):

$$u = k \operatorname{sech}(kx - k^3t + x_0), \quad (16)$$

where k is a free parameter, and the corresponding complex bright soliton of the KdV equation

$$u = k^2 \operatorname{sech}^2(kx - k^3t + x_0) - ik^2 \operatorname{sech}(kx - k^3t + x_0) \tanh(kx - k^3t + x_0) \quad (17)$$

by the complex Miura transform (9).

Case A.—We fix $c = d = 0$, and learn the two parameters a , b . The data-set is sampled in the spatio-temporal region $(x, t) \in [-10, 10] \times [-10, 10]$. Moreover, 10,000 sampling points will be used in the training process, and $k = 0.8$ in this example. A 6-layer neural network with 40 neurons per layer is used to learn system (15) to fit the exact solutions of two equations. For convenience, the initial value of all free parameters are set as 1. We choose 10,000 steps Adam and 20,000 steps L-BFGS optimizations to train the considered deep learning model. Case A in Table 2 exhibits the learning parameters about a , b , and their errors under two senses of the training data without a noise and with a 2% noise, which imply that the used deep learning method is effective. The training times are 609.30s and 645.68s, respectively. Moreover, the errors are exhibited in Figs. 3(b1-b4) for the cases without a noise and with a 2% noise, respectively.

Case B.—We learn all four parameters a , b , c , d . We used the same deep neural network method as Case A to study this case. Case B in Table 2 displays the learning parameters about a , b , c , d , and their errors under two senses of the training data without a noise and with a 2% noise, which imply that the used deep learning method is effective. The training times are 635.56s and 637.18s, respectively. Moreover, the errors are exhibited in Figs. 3(c1-c4) for the cases without a noise and with a 2% noise, respectively.

Case 2. Data-driven discovery of real Miura transform

We consider the generalized form of the real Miura transform (10) as

$$v = au_x + bu^2 + cuu_x + du_{xx}. \quad (18)$$

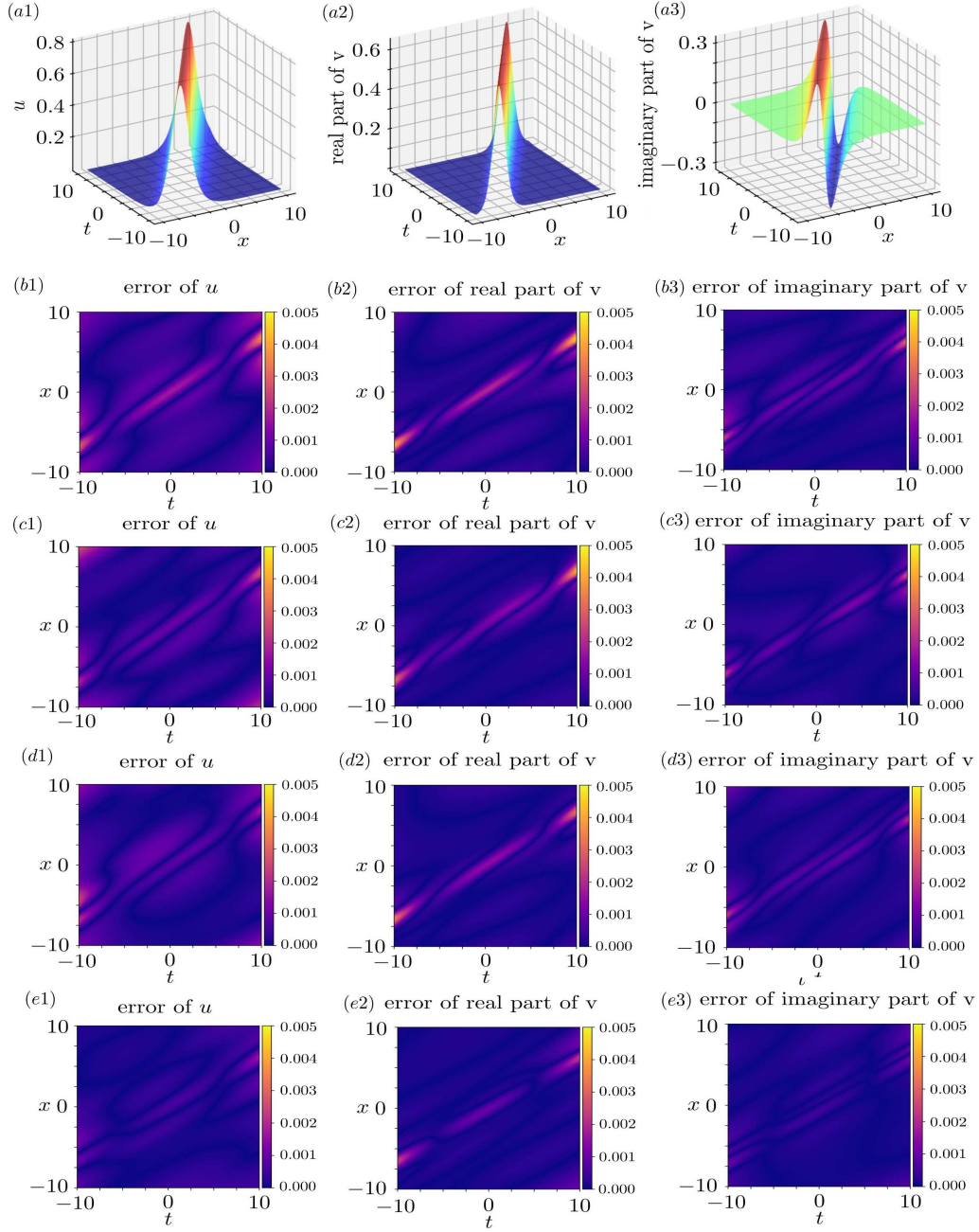


Figure 3: Data-driven complex Miura transform discovery. (a1) soliton (16), (a2, a3) real and imaginary parts of soliton (17). (b1-e3) Relative errors between exact solutions and neural network solutions: (b1-b3) Case A without a noise, (c1-c3) Case A with a 2% noise, (d1-d3) Case B without a noise, (e1-e3) Case B with a 2% noise. The relative \mathbb{L}^2 -norm errors of $u(x, t)$, $\text{Re}(v(x, t))$ and $\text{Im}(v(x, t))$ are (b1) $2.11\text{e-}3$, (b2) $2.71\text{e-}3$, (b3) $2.68\text{e-}3$, (c1) $1.69\text{e-}3$, (c2) $2.17\text{e-}3$, (c3) $2.16\text{e-}3$, (d1) $1.58\text{e-}3$, (d2) $2.00\text{e-}3$, (d3) $2.17\text{e-}3$, (e1) $9.43\text{e-}3$, (e2) $1.53\text{e-}3$, and (e3) $1.43\text{e-}3$, respectively.

where a, b, c, d are four real parameters to be determined. If $a = b = 1, c = d = 0$, then the transform (18)

reduces to the known real Miura transform (10).

In what follows, we would like to use the above-mentioned deep leaning scheme to discover these parameters a, b, c, d of the Miura transform (18) between the mKdV equation and KdV equation in two cases by considering the system

$$\begin{cases} u_t - 6u^2u_x + u_{xxx} = 0, \\ v_t + 6vv_x + v_{xxx} = 0, \\ v - au_x - bu^2 - cuu_x - du_{xx} = 0. \end{cases} \quad (19)$$

The training data-set is generated by a shock wave solution of the defocusing mKdV equation (12)

$$u(x, t) = k \tanh(kx + k^3t) \quad (20)$$

with a free real parameter $k \neq 0$, and the soliton solution of the KdV equation (13)

$$v(x, t) = 2k^2 \text{sech}^2(kx + 2k^3t) - k^2 \quad (21)$$

via the real Miura transform (10).

Case A.—We fix $c = d = 0$, and learn the two parameters a, b . The data-set is sampled in the spatio-temporal region $(x, t) \in [-3, 3] \times [-3, 3]$. Moreover, 10,000 sampling points will be used in the training process, and $k = 1$ in this example. A 7-layer neural network with 20 neurons per layer is used to learn system (19) to fit the exact solutions of two equations. For convenience, the initial value of all free parameters are set as 1. We choose 5,000 steps Adam and 5,000 steps L-BFGS optimizations to train the considered deep learning model. Case A in Table 3 exhibits the learning parameters about a, b , and their errors under two senses of the training data without a noise and with a 2% noise, which imply that the used deep learning method is effective. The training times are 374.40s and 407.44s, respectively. Moreover, the errors are exhibited in Figs. 4(b1-c3) for the cases without a noise and with a 2% noise, respectively.

Case B.—We learn all four parameters a, b, c, d . We used the same deep neural network method as Case A to study this case. Case B in Table 3 displays the learning parameters about a, b, c, d , and their errors under two senses of the training data without a noise and with a 2% noise, which imply that the used deep learning method is effective. The training times are 405.32s and 417.00s, respectively. Moreover, the errors are exhibited in Figs. 4(d1-e3) for the cases without a noise and with a 2% noise, respectively.

2.2 Data-driven discovery of mKdV equation via Miura transforms

2.2.1 Data-driven discovery of mKdV equation via the complex Miura transform

In this subsection, we would like to use the above-mentioned deep learning scheme to learn the mKdV equation through the complex Miura transform (9). The solution u of the mKdV equation (11) can not be explicitly expressed by the solution v of the KdV equation (13). The training data of u can not direct calculate by the data-set of v . So, we will use a neural network approximate u directly. Training loss TL_T brings u close to real solution.

We would like to consider the generalized form of the original mKdV equation (11)

$$u_t + au^2u_x + bu_{xxx} + cuu_{xx} + du^4 = 0 \quad (22)$$

to test the robustness of our scheme, where a, b, c, d are real-valued parameters to be determined.

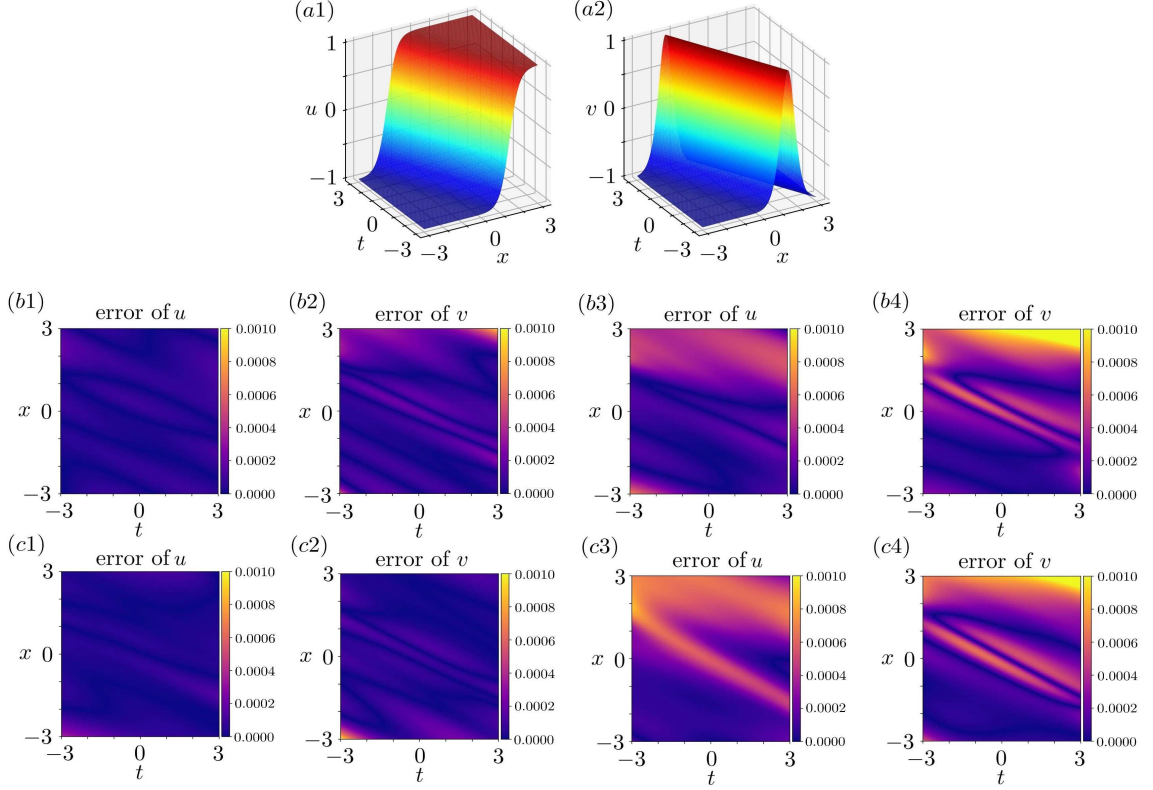


Figure 4: Data-driven discovery of real Miura transform. (a1) solution(20),(a2) soliton solution(21). (b1-e4) Relative errors between exact solutions and neural network solutions: (b1-b2) Case A without a noise, (b3-b4) Case A with a 2% noise,(c1-c2) Case B without a noise, (c3-c4) Case B with a 2% noise. The relative \mathbb{L}^2 -norm errors of $u(x, t)$ and $v(x, t)$ are (b1) $5.74\text{e-}5$, (b2) $1.44\text{e-}4$, (b3) $2.69\text{e-}4$, (b4) $4.42\text{e-}4$, (c1) $5.37\text{e-}5$, (c2) $9.37\text{e-}5$, (c3) $4.17\text{e-}4$, and (c4) $3.91\text{e-}4$, respectively.

We use the above-mentioned deep learning scheme to discover the parameters of the mKdV equation (22) via the complex Miura transform (9) and KdV equation (13) in two cases by considering the system

$$\begin{cases} u_t + au^2u_x + bu_{xxx} + cuu_{xx} + du^4 = 0, \\ v - iu_x - u^2 = 0. \end{cases} \quad (23)$$

Case A.—We fix $c = d = 0$, and learn the two parameters a, b . The training data-set is generated by the soliton (17) of the KdV equation. The data-set is sampled in the spatio-temporal region $(x, t) \in [-10, 10] \times [-5, 5]$. Moreover, 10,000 sampling points will be used in the training process, and $k = 0.8$ in this example. A 6-layers neural network with 40 neurons per layer is used to learn system (23) to fit the exact solutions of two equations. For convenience, the initial value of all free parameters are set as 1. We choose 10,000 steps Adam and 20,000 steps L-BFGS optimizations to train the considered deep learning model. Case A in Table 4 exhibits the learning parameters about a, b , and their errors under two senses of the training data without a noise and with a 2% noise, which imply that the used deep learning method is effective. The training times are 768.54s and 764.55s, respectively. Moreover, the errors are exhibited in Figs. 5(b1-b4) for the cases without a noise and with a 2% noise, respectively.

Table 4: Data-driven discovery of the mKdV equation (22) via system (23) with the complex Miura transform (9): a, b, c, d , and their errors, as well as the training times.

Case	a	b	c	d	
Exact	6	1	0	0	
A (no noise)	5.94175	0.98650	0	0	
A (2% noise)	5.90499	0.97883	0	0	
B (no noise)	5.96718	0.99260	1.88×10^{-3}	1.37×10^{-3}	
B (2% noise)	5.95149	0.98922	3.3×10^{-4}	-3.8×10^{-4}	
Case	error of a	error of b	error of c	error of d	time
A (no noise)	5.83×10^{-2}	1.35×10^{-2}	0	0	768.54s
A (2% noise)	9.50×10^{-2}	2.12×10^{-2}	0	0	764.55s
B (no noise)	3.28×10^{-2}	7.40×10^{-3}	1.88×10^{-3}	1.37×10^{-3}	742.11s
B (2% noise)	4.85×10^{-2}	1.08×10^{-2}	3.27×10^{-4}	3.80×10^{-4}	750.01s

Case B.—We learn all four parameters a, b, c, d . We used the same deep neural network method as Case A to study this case. Case B in Table 4 displays the learning parameters about a, b, c, d , and their errors under two senses of the training data without a noise and with a 2% noise, which imply that the used deep learning method is effective. The training times are 742.11s and 750.01s, respectively. Moreover, the errors are exhibited in Figs. 5(c1-c4) for the cases without a noise and with a 2% noise, respectively.

2.2.2 Data-driven discovery of mKdV equation via the real Miura transform

In this subsection, we would like to learn the mKdV equation through the real Miura transform (10). In general, the solution u of the mKdV equation (11) is very difficultly expressed by the solution v of the KdV equation (13). The training data of u can not be directly generated by the data-set of v . So, we will use a neural network to approximate u directly. The smaller training loss TL_T can make the trained \hat{u} close to real solution u .

We would like to consider the generalized form of the original mKdV equation given by Eq. (22) to test the robustness of our scheme. We use the above-mentioned deep learning scheme to discover the parameters of the mKdV equation (22) via the real Miura transform (10) and KdV equation (13) in two cases by considering the system

$$\begin{cases} u_t + au^2u_x + bu_{xxx} + cuu_{xx} + du^4 = 0, \\ v - u_x + u^2 = 0. \end{cases} \quad (24)$$

Case A.—We fix $c = d = 0$, and learn the two parameters a, b . The training data-set is generated by the soliton (21) of the KdV equation. The data-set is sampled in the spatio-temporal region $(x, t) \in [-3, 3] \times [-3, 3]$. Moreover, 10,000 sampling points will be used in the training process, and $k = 0.8$ in this example. A 7-layer neural network with 20 neurons per layer is used to learn system (24) to fit the exact solutions of two equations. For convenience, the initial value of all free parameters are set as 1. We choose 5,000 steps Adam and 5,000 steps L-BFGS optimizations to train the considered deep learning model. Case A in Table 5 exhibits the learning parameters about a, b , and their errors under two senses of the training data without a noise and with a 2% noise, which imply that the used deep learning method is effective. The training times are 203.41s and 178.44s,

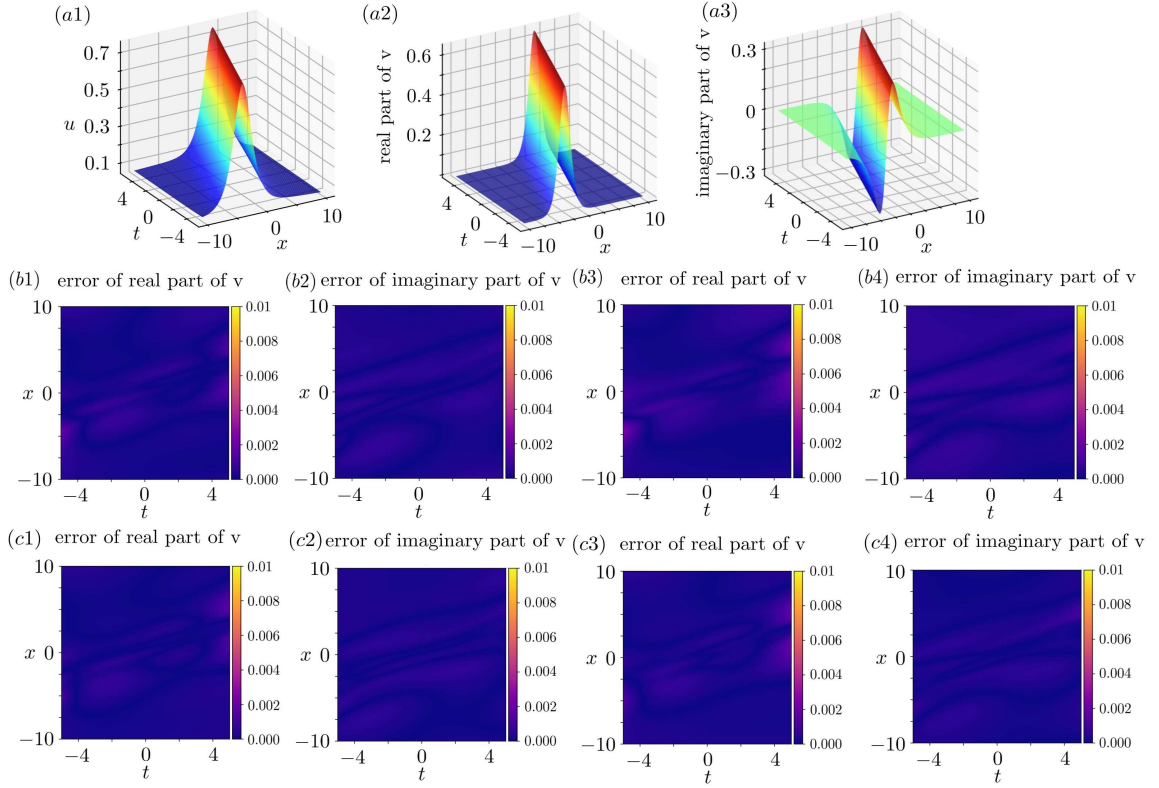


Figure 5: Data-driven discovery of the focusing mKdV equation via the complex Miura transform. (a1) trained soliton of mKdV equation, (a2-a3) real and imaginary parts of trained soliton of the KdV equation. (b1, b2) Case A without a nose, (b3, b4) Case A with a 2% noise, (c1, c2) Case B without a noise, (c3, c4) Case B with a 2% noise. The relative \mathbb{L}^2 -norm errors of $\text{Re}(v(x, t))$ and $\text{Im}(v(x, t))$ are (b1) 1.66×10^{-3} , (b2) 2.30×10^{-3} , (b3) 2.26×10^{-3} , (b4) 3.27×10^{-3} , (c1) 1.49×10^{-3} , (c2) 2.03×10^{-3} , (c3) 1.68×10^{-3} , and (c4) 1.92×10^{-3} , respectively.

respectively. Moreover, the errors are exhibited in Figs. 6(b1, b2) for the cases without a noise and with a 2% noise, respectively.

Case B.—We learn all four parameters a, b, c, d . We used the same deep neural network method as Case A to study this case. Case B in Table 5 displays the learning parameters about a, b, c, d , and their errors under two senses of the training data without a noise and with a 2% noise, which imply that the used deep learning method is effective. The training times are 178.08s and 163.98s, respectively. Moreover, the errors are exhibited in Figs. 6(b3, b4) for the cases without a noise and with a 2% noise, respectively.

3 The BT-enhanced scheme for data-driven PDE discovery

Some deep learning schemes about the PDE discovery usually only used the basic physical data (e.g., PDE solution data) and the possible forms of the presupposed PDEs (see, e.g., Ref. [44]). Sometime they are not effective. In this section, we will propose an enhanced scheme of PDE discovery based on the BTs. We can consider the BTs into two forms, including implicit and explicit forms to learn the soliton equations.

Table 5: Data-driven mKdV equation (22) discovery via system (24) with the real Miura transform (10): a, b, c, d , and their errors, as well as the training times.

Case	a	b	c	d	
Exact	-6	1	0	0	
Case A (no noise)	-5.98709	0.99742	0	0	
Case A (2% noise)	-5.97933	0.99527	0	0	
Case B (no noise)	-5.98739	0.99681	-0.00330	-0.00122	
Case B (2% noise)	-5.97631	0.99433	-0.00204	-0.00149	

Case	error of a	error of b	error of c	error of d	time
Case A (no noise)	1.29×10^{-2}	2.58×10^{-3}	0	0	203.41s
Case A (2% noise)	2.07×10^{-2}	4.73×10^{-3}	0	0	178.44s
Case B (no noise)	1.26×10^{-2}	3.19×10^{-3}	3.30×10^{-3}	1.22×10^{-3}	178.08s
Case B (2% noise)	2.37×10^{-2}	5.67×10^{-3}	2.04×10^{-3}	1.50×10^{-3}	163.98s

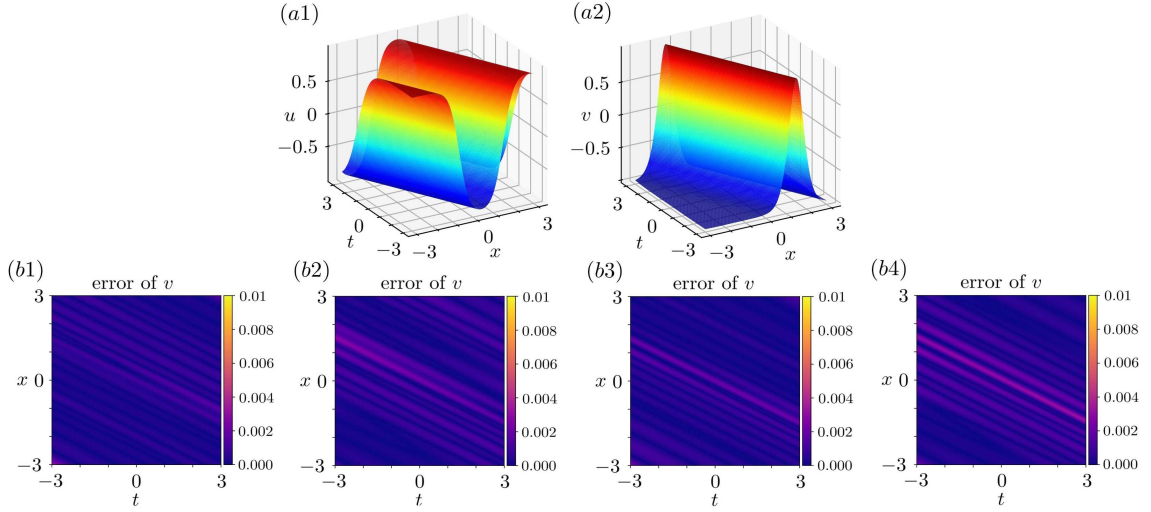


Figure 6: Data-driven discovery of the defocusing mKdV equation via the real Miura transform. (a1) trained soliton of mKdV equation, (a2) trained soliton of the KdV equation. (b1) Case A without a nose, (b2) Case A with a 2% noise, (b3) Case B without a noise, (b4) Case B with a 2% noise. The relative \mathbb{L}^2 -norm errors of $v(x, t)$ are (b1) 5.44×10^{-4} , (b2) 8.25×10^{-4} , (b3) 6.19×10^{-4} , and (b4) 9.64×10^{-4} , respectively.

3.1 The BT-enhanced deep learning scheme for PDE discovery

In this section, we will provide the framework of our scheme. The main idea about the PDE discovery in the previous works is to use the solution information, which may be generated by the experiment data-set or given data-set. But if we know the BT of the original equation, then we can find the higher accuracy of parameters in the original equation. The basic idea of this method is to add the high-order constraints to the training process, which are generated by the BTs.

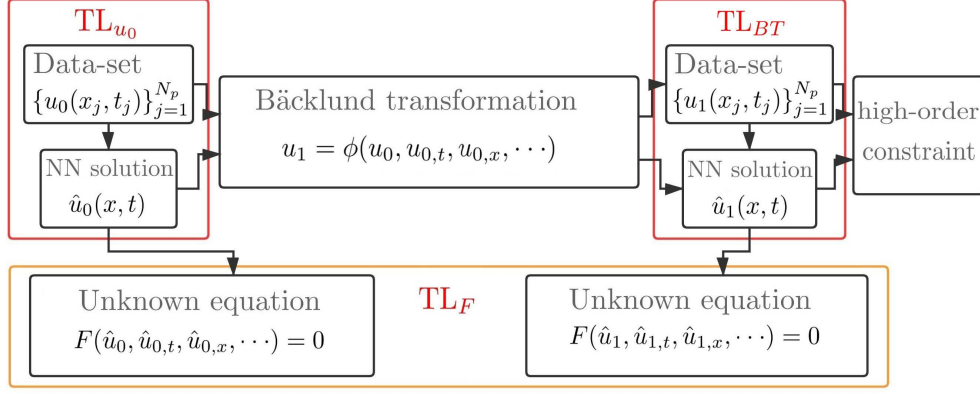


Figure 7: The BT-enhanced PDE discovery scheme for the explicit BTs.

We will discuss our scheme in two different cases. In the first case, the BT can be written as an explicit form. In the second case, the BT can be written only in an implicit form.

Case 1.—Fig 7 exhibits the case that the BT can be written as an explicit form. $\hat{u}_0(x, t)$ and $\hat{u}_1(x, t)$ are represented by some neural networks, such as the fully-connected neural networks or other kinds of neural networks. The data-set $\{u_0(x_j, t_j)\}_{j=1}^{N_p}$ arises from the experimental data or solution data. And the first-order data-set $\{u_1(x_j, t_j)\}_{j=1}^{N_p}$ is only calculated from the above data-set $\{u_0(x_j, t_j)\}_{j=1}^{N_p}$ by some BT. The unknown equations contain some parameters to be learned. The train loss contains the three parts: TL_{u_0} , TL_{BT} and TL_F , where TL_{u_0} and TL_{u_1} make the neural network model fit the data-set, and the TL_F makes the unknown equation approach to the exact form, which composed by the above neural network solution. If necessary, the high-order solutions can generate the stronger constraints. It is worth noting that the data-set $\{u_1(x_j, t_j)\}_{j=1}^{N_p}$ should be prepared before training.

The train loss TL contains the three parts: TL_{u_0} , TL_{BT} and TL_F , that is, $TL = TL_{u_0} + TL_{BT} + TL_F$, where

$$TL_{u_0} = \frac{1}{N_p} \sum_{j=1}^{N_p} |u_0(x_j, t_j) - \hat{u}_0(x_j, t_j)|^2, \quad (25)$$

$$TL_{BT} = \frac{1}{N_p} \sum_{j=1}^{N_p} |BT(u_0(x_j, t_j)) - \hat{u}_1(x_j, t_j)|^2, \quad (26)$$

$$TL_F = \frac{1}{N_p} \sum_{j=1}^{N_p} \left(|F(\hat{u}_0(x_j, t_j))|^2 + |F(\hat{u}_1(x_j, t_j))|^2 \right) \quad (27)$$

in which TL_{u_0} and TL_{BT} make the neural network model fit the data-set, TL_F makes the unknown equation approach to the exact form, which composed by above neural network solutions \hat{u}_0 and \hat{u}_1 . If necessary, high-order solution can be used to obtain the stronger constraints. For instance, if we use $\{u_0(x_j, t_j)\}_{j=1}^{N_p}$, $\{BT(u_0(x_j, t_j))\}_{j=1}^{N_p}$ and 2-order data-set $\{BT^2(u_0(x_j, t_j))\}_{j=1}^{N_p}$ to train our model to obtain the neural network solutions $\hat{u}_j (j = 0, 1, 2)$. The losses TL_{BT} and TL_F in the TL are replaced by

$$TL_{BT^2} = \frac{1}{N_p} \sum_{j=1}^{N_p} \left(|BT(u_0(x_j, t_j)) - \hat{u}_1(x_j, t_j)|^2 + |BT^2(u_0(x_j, t_j)) - \hat{u}_2(x_j, t_j)|^2 \right), \quad (28)$$

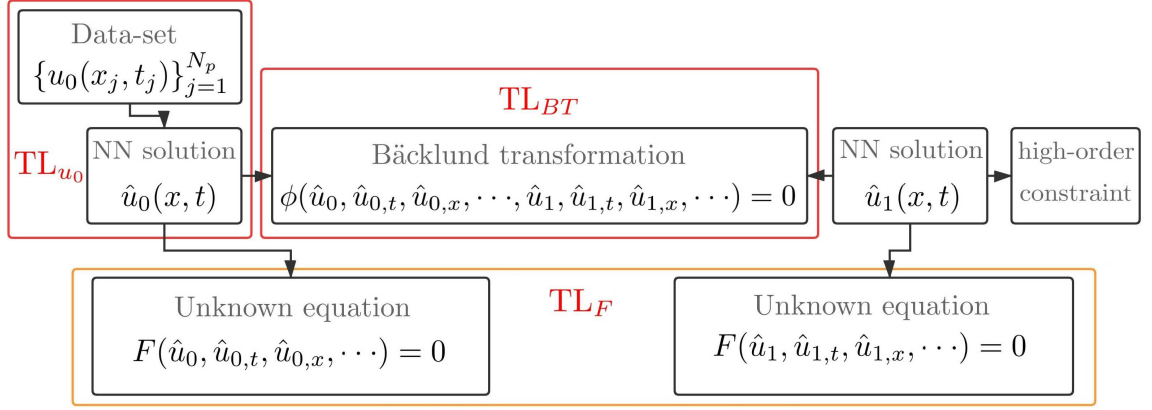


Figure 8: The BT-enhanced PDE discovery scheme for the implicit BTs.

and

$$\text{TL}_F = \frac{1}{N_p} \sum_{j=1}^{N_p} \left(|F(\hat{u}_0(x_j, t_j))|^2 + |F(\hat{u}_1(x_j, t_j))|^2 + |F(\hat{u}_2(x_j, t_j))|^2 \right). \quad (29)$$

Case 2.—Fig 8 displays the case that the BT can be written as an implicit form. Since the BT is an implicit form, thus we can not get the data-set of $u_1(x, t)$. We use the training loss TL_{BT} to obtain the approximated neural network solution $\hat{u}_1(x, t)$. And the approximated neural network solution $\hat{u}_0(x, t)$ can still be trained by the data-set $\{u_0(x_j, t_j)\}_{j=1}^{N_p}$ through TL_{u_0} . The unknown equation will be learned by TL_F . The correct equation will be found more precise by the above two schemes. These models are trained by the efficient Adam optimization algorithm and L-BFGS optimization algorithm.

The loss function of this scheme is

$$\text{TL} = \text{TL}_{u_0} + \text{TL}_{BT} + \text{TL}_F, \quad (30)$$

where

$$\text{TL}_{u_0} = \frac{1}{N_p} \sum_{j=1}^{N_p} |u_0(x_j, t_j) - \hat{u}_0(x_j, t_j)|^2, \quad (31)$$

$$\text{TL}_{BT} = \frac{1}{N_p} \sum_{j=1}^{N_p} |\phi(\hat{u}_0(x_j, t_j), \hat{u}_1(x_j, t_j))|^2, \quad (32)$$

$$\text{TL}_F = \frac{1}{N_p} \sum_{j=1}^{N_p} \left(|F(\hat{u}_0(x_j, t_j))|^2 + |F(\hat{u}_1(x_j, t_j))|^2 \right) \quad (33)$$

The exact equation will be found more precise by the above scheme. If one wants to obtain the higher accuracy of unknown equations, an additional neural network solution \hat{u}_2 should be added. The losses TL_{BT} and TL_F in the TL are replaced by

$$\text{TL}_{BT^2} = \frac{1}{N_p} \sum_{j=1}^{N_p} \left(|\phi(\hat{u}_0(x_j, t_j), \hat{u}_1(x_j, t_j))|^2 + |\phi(\hat{u}_1(x_j, t_j), \hat{u}_2(x_j, t_j))|^2 \right) \quad (34)$$

Table 6: Comparisons of PINNs and BT-enhanced scheme for the data-driven mKdV equation discovery.

Case	a	error of a	b	error of b	c	error of c	d	error of d
Exact	6	0	1	0	0	0	0	0
A (PINNs)	5.63392	0.366	0.90826	0.0917	0	0	0	0
A (PINNs 2%)	5.60595	0.394	0.90041	0.0996	0	0	0	0
A (PINNs 5%)	5.56262	0.437	0.89004	0.110	0	0	0	0
A (PINNs 10%)	5.58002	0.420	0.89078	0.109	0	0	0	0
A (PINNs 20%)	3.64644	2.35356	0.45905	0.541	0	0	0	0
B (PINNs)	5.58765	0.412	0.90205	0.0979	-0.02825	0.0282	-0.01493	0.0149
B (PINNs 2%)	5.80756	0.192	0.95514	0.0449	-0.02467	0.0247	-0.02322	0.0232
B (PINNs 5%)	5.74998	0.250	0.94189	0.0581	-0.01166	0.0117	-0.01847	0.0185
B (PINNs 10%)	5.63770	0.362	0.91263	0.0874	-0.00343	0.00343	-0.01174	0.0117
B (PINNs 20%)	4.86428	1.14	0.73158	0.268	-0.02057	0.0206	-0.00608	0.00608
A (BTE)	6.00973	9.73×10^{-3}	1.00123	1.23×10^{-3}	0	0	0	0
A (BTE 2%)	5.97970	2.03×10^{-2}	0.99380	6.20×10^{-3}	0	0	0	0
A (BTE 5%)	5.98296	1.70×10^{-2}	0.99231	7.69×10^{-3}	0	0	0	0
A (BTE 10%)	5.99462	5.38×10^{-3}	0.99104	8.96×10^{-3}	0	0	0	0
A (BTE 20%)	5.97702	2.30×10^{-2}	0.97901	2.10×10^{-2}	0	0	0	0
B (BTE)	5.99109	8.91×10^{-3}	0.99804	1.96×10^{-3}	0.00086	8.57×10^{-4}	0.00110	1.10×10^{-3}
B (BTE 2%)	5.99943	5.72×10^{-4}	0.99818	1.82×10^{-4}	0.00013	1.35×10^{-4}	0.00028	2.80×10^{-4}
B (BTE 5%)	5.98173	1.83×10^{-2}	0.99214	7.86×10^{-4}	0.00024	2.38×10^{-4}	0.00016	1.62×10^{-4}
B (BTE 10%)	5.98347	1.65×10^{-2}	0.98876	1.12×10^{-2}	-0.00063	6.26×10^{-4}	-0.00142	1.42×10^{-3}
B (BTE 20%)	5.98058	1.94×10^{-2}	0.97879	2.12×10^{-2}	-0.00178	1.78×10^{-3}	-0.00305	3.05×10^{-3}

and

$$\text{TL}_F = \frac{1}{N_p} \sum_{j=1}^{N_p} \left(|F(\hat{u}_0(x_j, t_j))|^2 + |F(\hat{u}_1(x_j, t_j))|^2 + |F(\hat{u}_2(x_j, t_j))|^2 \right). \quad (35)$$

In the two above schemes, if we only use \hat{u}_0 and \hat{u}_1 to train the neural network, then we call it 1-fold BT-enhanced (BTE) scheme. And if we use \hat{u}_0 , \hat{u}_1 and \hat{u}_2 in the training process, we call it a 2-fold BTE scheme. All schemes are trained by the efficient Adam and L-BFGS optimization algorithms.

In what follows, we will display two examples to show the validity of our schemes. The first example is to learn the mKdV equation based on the explicit BT (alias Darboux transform (DT)) of the mKdV equation (36). The second example is to study the s-G equation via the implicit aBT (5).

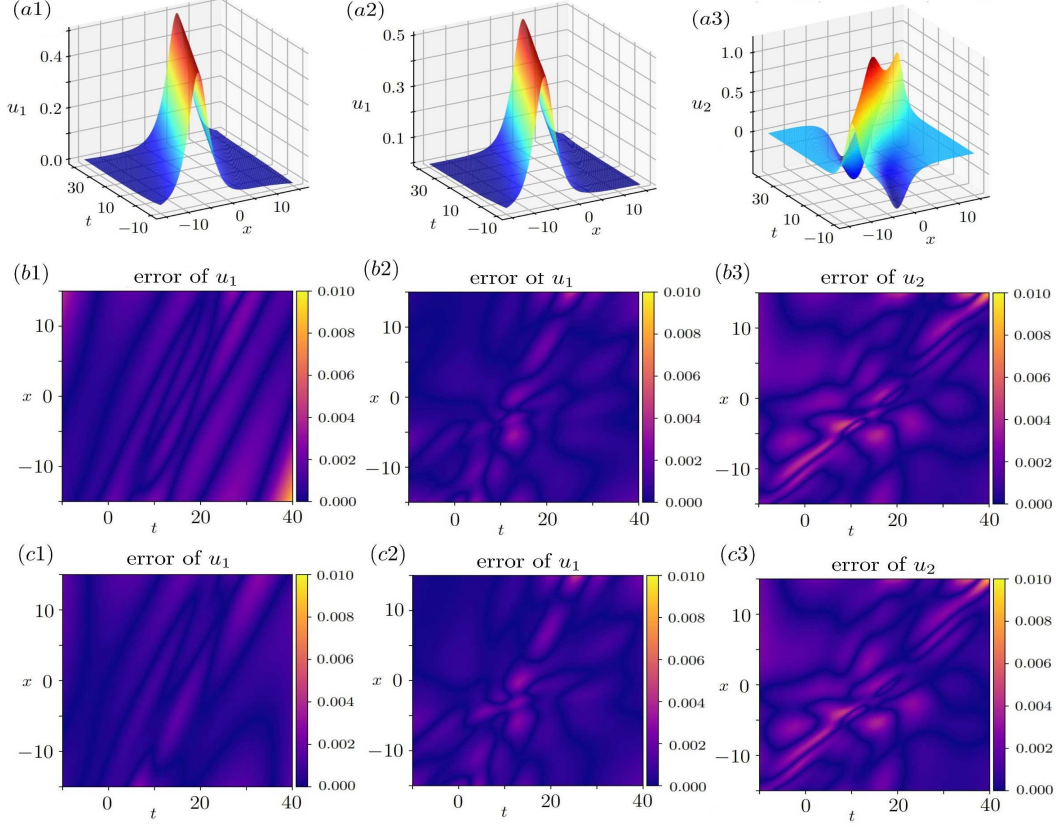


Figure 9: Focusing mKdV equation. (a1) trained one-soliton solution via PINNs and (a2, a3) trained one- and two-soliton solutions via the BT-enhanced PDE scheme. (b1-c3) absolute errors: (b1) PINNs learning Case A with a 5% noise, (b2-b3) BT-enhanced PDE scheme learning Case A with a 5% noise, (c1) PINNs learning Case B with a 5% noise, (c2-c3) BT-enhanced PDE scheme learning Case B with a 5% noise. The relative \mathbb{L}^2 -norm errors of u_1 and u_2 are: (b1) 6.61×10^{-3} , (b2) 3.71×10^{-3} , (b3) 4.61×10^{-3} , (c1) 5.81×10^{-2} , (c2) 3.80×10^{-3} , and (c3) 4.41×10^{-3} , respectively. The training times are (b1) 132.14s, (b2-b3) 302.67s, (c1) 135.95s, and (c2-c3) 285.60s, respectively.

3.2 Data-driven discovery of mKdV equation via the explicit BT/DT

The focusing mKdV equation (11) possesses the BT/DT [63]

$$u_{n+1} = u_n + \frac{4\lambda\psi}{1+\psi^2}, \quad \psi = \frac{\Phi_{22}(x, t, \lambda) + \mu\Phi_{21}(x, t, \lambda)}{\Phi_{12}(x, t, \lambda) + \mu\Phi_{11}(x, t, \lambda)} \quad (36)$$

with a free parameter μ , where

$$\Phi = \begin{pmatrix} \Phi_{11}(x, t, \lambda) & \Phi_{12}(x, t, \lambda) \\ \Phi_{21}(x, t, \lambda) & \Phi_{22}(x, t, \lambda) \end{pmatrix}$$

is the basic solution of the Lax pair of the mKdV equation (11)

$$\Phi_x = \begin{pmatrix} \lambda & u \\ -u & -\lambda \end{pmatrix} \Phi, \quad \Phi_t = \begin{pmatrix} -2\lambda(2\lambda^2 + u^2) & -2\lambda(2u\lambda + u_x) - 2u^3 - u_{xx} \\ 2\lambda(2u\lambda - u_x) + 2u^3 + u_{xx} & 2\lambda(2\lambda^2 + u^2) \end{pmatrix} \Phi \quad (37)$$

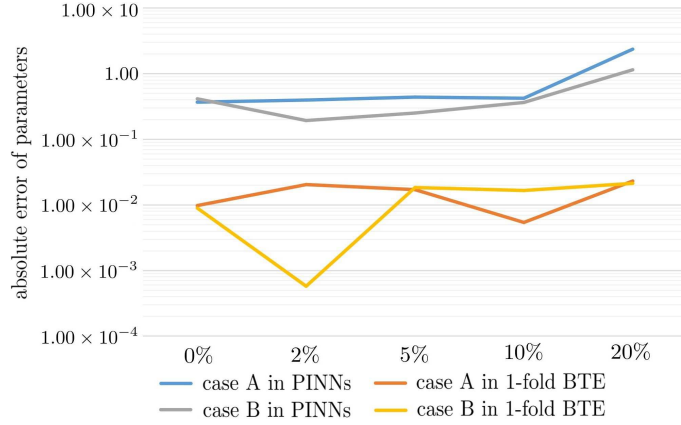


Figure 10: Error comparisons between the BTE and PINNs schemes for the mKdV equation. The vertical axis is the maximum of the absolute errors of all parameters.

with $\lambda \in \mathbb{C}$ being a spectral parameter, and u an initial solution of the mKdV equation (11).

By using the above DT (36) with $u_0 = 0$, $\mu = e^{2\alpha_1}$ and $\lambda = \lambda_1$, one can obtain the one-soliton solution of the mKdV equation (11)

$$u_1(x, t) = 2\lambda_1 \text{sech}(2\lambda_1 x - 8\lambda_1^3 t + 2\alpha_1) \quad (38)$$

Further, one can use the DT (36) with u_1 given by Eq. (38), $\mu = e^{2\alpha_2}$ and $\lambda = \lambda_2$, to find the 2-soliton solution of the mKdV equation (11)

$$u_2(x, t) = \frac{2(\lambda_2^2 - \lambda_1^2)(\lambda_2 \cosh(v_1) - \lambda_1 \cosh(v_2))}{(\lambda_1^2 + \lambda_2^2) \cosh(v_1) \cosh(v_2) - 2\lambda_1 \lambda_2 (1 + \sinh(v_1) \sinh(v_2))}, \quad (39)$$

where $v_j = 2\lambda_j x - 8\lambda_j^3 t + 2\alpha_j$, ($j = 1, 2$), and $\lambda_2 > \lambda_1 > 0$. In this example, we take $\lambda_1 = \frac{1}{4}$, $\lambda_2 = \frac{1}{3}$, $\alpha_1 = 1$, and $\alpha_2 = 2$. According to the homogeneity principle of mKdV equation, we add two disturbance terms u^4 , uu_{xx} to the mKdV equation to generate the generalized form

$$u_t + au^2 u_x + bu_{xxx} + cu^4 + duu_{xx} = 0, \quad (40)$$

which is used to examine the robustness of the scheme, where a , b , c , and d are real-valued parameters to be determined.

In what follows, we would like to use the above-mentioned BT-enhanced PDE discovery scheme given by Fig. 7 to discover these parameters a , b , c , d of the mKdV equation (40) in two cases by considering the system

$$\begin{cases} u_t + au^2 u_x + bu_{xxx} + cu^4 + duu_{xx} = 0, \\ u_2 - u_1 - \frac{4\lambda\psi}{1 + \psi^2} = 0, \end{cases} \quad (41)$$

The training data-set is generated by the soliton solution (38) of the focusing mKdV equation (11). To compare our scheme with the known PINNs scheme [44], which is trained by considering Eq. (40) with the initial data generating from u_1 .

Case A.—We fix $c = d = 0$, and learn two parameters a and b . We take the initial values of a , b as $a = b = 1$. The training data-set is generated by not only the one-soliton solution (38) but also the two-soliton solution (39)

Table 7: Comparisons of PINNs and BT-enhanced PDE scheme for the data-driven s-G equation discovery.

Case	a	error of a	b	error of b
Exact	1	0	0	0
PINNs (no noise)	0.99991	9.18×10^{-5}	-0.00002	2.16×10^{-5}
PINNs (2% noise)	1.00051	5.13×10^{-4}	-0.00005	5.30×10^{-5}
PINNs (5% noise)	1.00128	1.28×10^{-3}	0.00002	1.58×10^{-5}
PINNs (10% noise)	1.00239	2.39×10^{-3}	-0.00019	1.90×10^{-4}
PINNs (20% noise)	1.00466	4.66×10^{-3}	-0.00041	4.13×10^{-4}
1-fold BTE (no noise)	0.99996	4.15×10^{-5}	0.00001	1.30×10^{-5}
1-fold BTE (2% noise)	1.00020	1.98×10^{-4}	-0.00000	7.21×10^{-6}
1-fold BTE (5% noise)	1.00057	5.70×10^{-4}	-0.00003	2.97×10^{-5}
1-fold BTE (10% noise)	1.00108	1.07×10^{-3}	-0.00007	6.46×10^{-5}
1-fold BTE (20% noise)	1.00218	2.18×10^{-3}	-0.00010	9.67×10^{-5}
2-fold BTE (no noise)	0.99984	1.59×10^{-4}	-0.00004	4.05×10^{-5}
2-fold BTE (2% noise)	1.00003	3.42×10^{-5}	0.00002	1.54×10^{-5}
2-fold BTE (5% noise)	1.00036	3.58×10^{-4}	-0.00004	3.72×10^{-5}
2-fold BTE (10% noise)	1.00081	8.08×10^{-4}	-0.00001	1.10×10^{-5}
2-fold BTE (20% noise)	1.00146	1.46×10^{-3}	-0.00011	1.12×10^{-4}

of the mKdV equation. The training data-set is sampled in the region $(x, t) \in [-15, 15] \times [-10, 40]$, and 10,000 sampling points are used in the training processes. For the BT-enhanced PDE discovery scheme given by Fig. 7, two solitons u_1 and u_2 are approximated by using a 6-layer neural network with 40 neurons per layer, and 5,000 steps Adam and 5,000 steps L-BFGS optimizations are chosen. We use the usual PINNs with the training data arising from the one-soliton solution u_1 , and our scheme with the same neural networks to learn two parameters a , b , respectively, such that Case A of Table 6 displays the learning results and their errors under two senses of the training data without a noise and with the differential 2%, 5%, 10%, 20% noises. Figs. 9 and 10 exhibit the errors of training results of all conditions, which imply that our scheme is better than the PINNs scheme for the same training steps. That is to say, except for the one-soliton data arising from u_1 , the used more data u_2 generated from the DT (36) can make the errors of learning results smaller in the BT-enhanced PDE discovery scheme given by Fig. 7.

Case B.—We learn all four parameters a , b , c , d in Eq. (40). We used the same BT-enhanced PDE discovery scheme given by Fig. 7 as Case A and PINNs to study this case, respectively. For the two senses of the training data without a noise and with the differential 2%, 5%, 10%, 20% noises, Case B in Table 6 displays the learning parameters about a , b , c , d , and their errors via our scheme and the known PINNs. The results imply that the BT-enhanced PDE discovery scheme given by Fig. 7 is more effective (see Figs. 9 and 10).

3.3 Data-driven discovery of s-G equation via the implicit aBT

We know that the s-G equation (4) has the aBT (5), which can be used to generate its new solution $u'(x, t)$. In what follows, we will utilize this aBT to find the high precision s-G equation. Meanwhile, we will compare

the result between the BT-enhanced PDE discovery scheme given by Fig. 8 and known PINNs scheme [44]. We consider the aBT of the generalized s-G equation

$$u_{xt} = a \sin u + b \cos u, \quad (42)$$

where a, b are parameters to be determined. As $a = 1, b = 0$, Eq. (42) reduces to the known aBT of the s-G equation [57].

In what follows, we would like to use the above-mentioned BT-enhanced PDE discovery scheme given by Fig. 8 to discover these parameters a, b of the generalized s-G equation (42) in two cases by considering the system

$$\begin{cases} u_{xt} - a \sin u - b \cos u = 0, \\ u'_x = u_x - 2\beta \sin\left(\frac{u + u'}{2}\right), \\ u'_t = -u_t + \frac{2}{\beta} \sin\left(\frac{u - u'}{2}\right). \end{cases} \quad (43)$$

The training data-set is generated by the breather solution (8) of the s-G equation (4). To compare our scheme with the known PINNs scheme, which is trained by considering Eq. (42) with the initial data generating from the breather solution (8).

The training data are generated by the breather solution (8). The 10,000 sampling points are selected in $\{(x, t) | (x, t) \in [-10, 10] \times [-5, 5]\}$. The 5,000 steps Adam and 5,000 steps L-BFGS optimizations will be used in each case. the trained solution \hat{u}_0, \hat{u}_1 , and \hat{u}_2 are represented by one 6-layer neural network with 40 neurons per layer. \hat{u}_0 will approach to real solution (8), and \hat{u}_1, \hat{u}_2 just are neural network solutions. Fig. 11 displays the breather-like profiles of \hat{u}_0, \hat{u}_1 , and \hat{u}_2 . Fig. 12 exhibits the training results of all conditions, where the vertical axis represents the max error of b and c , and the horizontal axis denotes the different error of training data. As a result, we find that our scheme is almost always better than the PINNs scheme for the same training steps.

4 Conclusions and discussions

In conclusion, we have established the deep neural network learning algorithms to discover BTs and soliton evolution equations. Three types of BTs are used to investigate the availability of our scheme such as the aBT of the sine-Gordon equation, complex/real Miura transforms between the defocusing/focusing mKdV equation and KdV equation, as well as the DT of the focusing mKdV equation. Moreover, we also compare our scheme with the known PINNs such that our scheme is more effective in the study of data-driven discovery of soliton equations via BTs. The idea can also be extended to other types of BTs and nonlinear PDEs containing physically interesting soliton equations.

Acknowledgements

This work is supported by the NSFC under Grant Nos. 11925108 and 11731014.

References

- [1] J. S. Russell, Report on waves, Rep. 14th Meeting of the British Assoc. for the Advancement of Science, John Murray, London, 1844, pp. 311-390.
- [2] N. J. Zabusky, M. D. Kruskal, Interaction of “solitons” in a collisionless plasma and the recurrence of initial states, Phys. Rev. Lett. 15 (1965) 240-243.

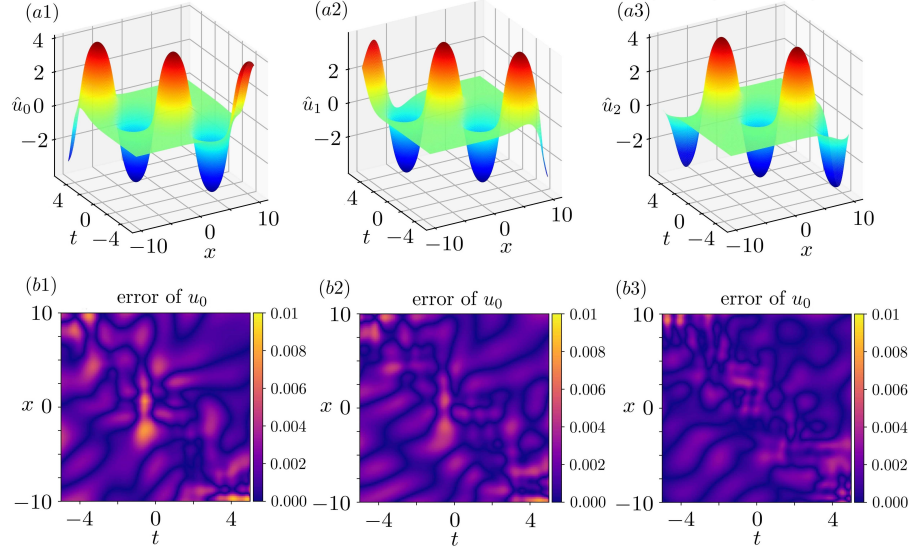


Figure 11: (a1-a3) Three neural network solutions of s-G equation via the 2-fold BTE scheme. (b1-b3) absolute errors of u_1 with a 2% noise: (b1) PINNs scheme, (b2) 1-fold BTE scheme, (b3) 2-fold BTE scheme. The relative \mathbb{L}^2 -norm errors of u_1 and training times are (b1) 1.51×10^{-3} , 123.20s, (b2) 1.33×10^{-3} , 343.72s, (b3) 1.01×10^{-3} , 505.11s, respectively.

- [3] D. J. Korteweg, G. de Vries, On the change of form of long waves advancing in a rectangular canal, and on a new type of long stationary waves, *Philos. Mag.* 39 (1895) 422-443.
- [4] G. L. Lamb Jr, *Elements of soliton theory* (Wiley, New York, 1980).
- [5] M. J. Ablowitz, P. A. Clarkson, *Solitons, nonlinear evolution equations and inverse scattering* (Cambridge University Press, 1991).
- [6] A. Hasegawa, Y. Kodama, *Solitons in Optical Communications* (Oxford University Press, Oxford, 1995).
- [7] N. Akhmediev, A. Ankiewicz, *Solitons: Nonlinear Pulses and Beams* (Chapman and Hall, London, 1997).
- [8] G.P. Agrawal, *Nonlinear Fiber Optics* (5th ed.) (Academic Press, New York, 2012).
- [9] L. Pitaevskii and S. Stringari, *Bose-Einstein Condensation* (Oxford University Press, Oxford, 2003).
- [10] C. Kharif, E. Pelinovsky, and A. Slunyaev, *Rogue Waves in the Ocean* (Springer, New York, 2009).
- [11] A. Osborne, *Nonlinear Ocean Waves and the Inverse Scattering Transform* (Elsevier, New York, 2010).
- [12] J. Yang, *Nonlinear Waves in Integrable and Nonintegrable Systems* (SIAM, 2010).
- [13] A. V. Bäcklund, Einiges über Curven und Flächentransformationen, *Lund Universitets Arsskrift* 10 (1875).
- [14] G. Darboux, On a proposition relative to linear equations, *Comptes Rendus Acad. Sci.* 94 (1882) 1456-1459.
- [15] R. Miura (ed.), *Bäcklund Transformations* (Springer, New York 1976).
- [16] G. L. Lamb Jr, Bäcklund transformations for certain nonlinear evolution equations, *J. Math. Phys.* 15 (1974) 2157.
- [17] C. Rogers, and W. R. Shadwick, *Bäcklund transformations and their application* (Academic Press, New York, 1982).
- [18] V. B. Matveev and M. A. Salle *Darboux transformations and solitons* (Springer, 1991).

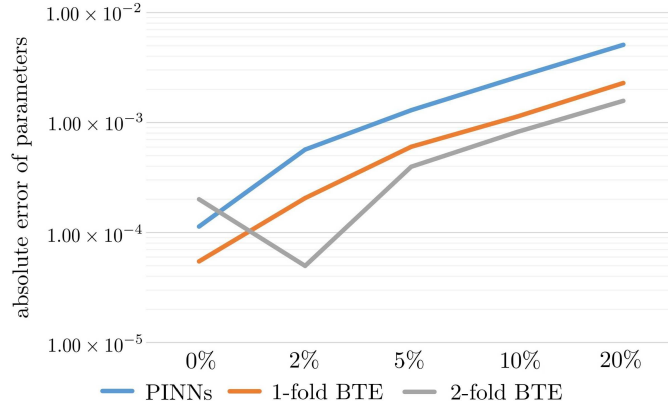


Figure 12: Error comparisons between the BTE scheme and PINNs for the sine-Gordon equation via the implicit aBT. The vertical axis is the maximum of the absolute errors of all parameters.

- [19] C. Rogers and W. K. Schief, *Bäcklund and Darboux transformations: geometry and modern applications in soliton theory* (Cambridge University Press, 2002).
- [20] G. W. Bluman and S. Kumei, *Symmetries and differential equations* (Springer, New York, 1989).
- [21] P. J. Olver, *Applications of Lie groups to differential equations* (Springer, New York, 2000).
- [22] R. Hirota, *The direct method in soliton theory* (Cambridge University Press, 2004).
- [23] G. W. Bluman, A. F. Cheviakov, and S. C. Anco, *Applications of symmetry methods to partial differential equations* (New York: Springer, 2010).
- [24] E. Hopf, The partial differential equation $u_t + uu_x = u_{xx}$, *Commun. Pure Appl. Math.* 3 (1950) 201.
- [25] J D. Cole, On a quasi-linear parabolic equations occurring in aerodynamics, *Quart. J. Appl. Math.* 9 (1951) 225.
- [26] C. S. Gardner, J. M. Greene, M. D. Kruskal, R. M. Miura, Method for solving the Korteweg-de Vries equation, *Phys. Rev. Lett.* 19 (1967) 1095-1097.
- [27] P. D. Lax, Integrals of nonlinear equations of evolution and solitary wave, *Commun. Pure Appl. Math.* 21 (1968) 467-490.
- [28] R. M. Miura, Korteweg-de Vries equation and generalizations. I. A remarkable explicit nonlinear transformation, *J. Math. Phys.* 9 (1968) 1202-1204.
- [29] I. Goodfellow, Y. Bengio, A. Courville, *Deep learning* (MIT Press, 2016).
- [30] Y. LeCun, Y. Bengio, G. Hinton, Deep learning, *Nature* 521 (2015) 436.
- [31] B.M. Lake, R. Salakhutdinov, J.B. Tenenbaum, Human-level concept learning through probabilistic program induction, *Science* 350 (2015) 1332-1338.
- [32] A. Krizhevsky, I. Sutskever, G.E. Hinton, Imagenet classification with deep convolutional neural networks, in: *Advances in Neural Information Processing Systems*, 2012, pp. 1097-1105.
- [33] B. Alipanahi, A. Delong, M.T. Weirauch, B.J. Frey, Predicting the sequence specificities of DNA- and RNA-binding proteins by deep learning, *Nat. Biotechnol.* 33 (2015) 831-838.
- [34] P. Larranaga, D. Atienza, J. Diaz-Rozo, A. Ogbechie, C. E. Puerto-Santana, C. Bielza, *Industrial Applications of Machine Learning* (CRC Press, 2019).

- [35] P. Johri, J. K. Verma, S. Paul (ed.) *Applications of Machine Learning* (Springer, New York, 2020).
- [36] M. Dissanayake and N. Phan-Thien. Neural-network-based approximations for solving partial differential equations, *Commun. Numer. Meth. Eng.* 10 (1994) 195-201.
- [37] I. E. Lagaris, A. Likas, and D. I. Fotiadis, Artificial neural networks for solving ordinary and partial differential equations, *IEEE transactions on Neural Networks*, 9 (1998) 987-1000.
- [38] I. E. Lagaris, A. C. Likas, and G. D. Papageorgiou. Neural-network methods for boundary value problems with irregular boundaries, *IEEE Transactions on Neural Networks*, 11 (2000) 1041-1049.
- [39] S.H. Rudy, S.L. Brunton, J.L. Proctor, and J. N. Kutz, Data-driven discovery of partial differential equations, *Sci. Adv.* 3 (2017) e1602614.
- [40] J. Sirignano and K. Spiliopoulos, DGM: A deep learning algorithm for solving partial differential equations, *J. Comput. Phys.* 375 (2018) 1339-1364.
- [41] J. Han, A. Jentzen, and W. E, Solving high-dimensional partial differential equations using deep learning, *PNAS* 115 (2018) 8505-8510.
- [42] Y. Bar-Sinai, S. Hoyer, J. Hickey, and M.P. Brenner, Learning data-driven discretizations for partial differential equations, *PNAS* 116 (2019) 15344-15349.
- [43] M. Raissi and G.E. Karniadakis, Hidden physics models: machine learning of nonlinear partial differential equations, *J. Comput. Phys.* 357 (2018) 125-141.
- [44] M. Raissi, P. Perdikaris, and G. E. Karniadakis. Physics-informed neural networks: A deep learning framework for solving forward and inverse problems involving nonlinear partial differential equations, *J. Comput. Phys.* 378 (2019) 686.
- [45] M. Raissi, A. Yazdani, and G. E. Karniadakis, Hidden fluid mechanics: Learning velocity and pressure fields from flow visualizations, *Science* 367 (2020) 1026-1030.
- [46] L. Lu, X. Meng, Z. Mao, and G. E. Karniadakis, DeepXDE: A deep learning library for solving differential equations, *SIAM Rev.* 63 (2021) 208-228..
- [47] Z. Mao, A. D. Jagtap, and G. E. Karniadakis, Physics-informed neural networks for high-speed flows, *Comput. Meth. Appl. Mech. Eng.* 360 (2020) 112789.
- [48] Z. Zhou and Z. Yan, Solving forward and inverse problems of the logarithmic nonlinear Schrödinger equation with PT-symmetric harmonic potential via deep learning, *Phys. Lett. A* 387 (2021) 127010.
- [49] L. Wang and Z. Yan, Data-driven rogue waves and parameter discovery in the defocusing NLS equation with a potential using the PINN deep learning, *Phys. Lett. A* 404 (2021) 127408 (arXiv: 2012.09984 (2020)).
- [50] L. Wang and Z. Yan, Data-driven peakon and periodic peakon travelling wave solutions of some nonlinear dispersive equations via deep learning, 2021, arXiv:2101.04371.
- [51] Z. Zhou and Z. Yan, Deep learning neural networks for the third-order nonlinear Schrödinger equation: Bright solitons, breathers, and rogue waves, *Commun. Theor. Phys.* 73 (2021) 105006.
- [52] G. Pang, L. Lu, and G. E. Karniadakis. fPINNs: Fractional physics-informed neural networks, *SIAM J. Sci. Comput.* 41 (2019) A2603-A2626.
- [53] D. Zhang, L. Guo, and G. E. Karniadakis, Learning in modal space: Solving time-dependent stochastic pdes using physics-informed neural networks, *SIAM J. Sci. Comput.* 42 (2020) A639-A665.
- [54] M. Stein, Large sample properties of simulations using Latin hypercube sampling, *Technometrics* 29 (1987) 143-151.
- [55] D. Kingma, J. Ba, Adam: a method for stochastic optimization, 2014, arXiv:1412.6980.

- [56] D.C. Liu, J. Nocedal, On the limited memory BFGS method for large scale optimization, *Math. Program.* 45 (1989) 503-528.
- [57] J.Frenkel, T. Kontorova, On the theory of plastic deformation and twinning, *J. Phys. USSR* 1 (1939) 137.
- [58] J. Rubinstein, Sine-Gordon equation, *J. Math. Phys.* 11(1970) 258.
- [59] A. Barone, F. Esposito, C. J. Magee, and A. C. Scott, Theory and applications of the sine-Gordon equation, *Riv. Nuovo Cimento* 1 (1971) 227.
- [60] P. J. Caudrey, J. C. Eilbeck, J. D. Gibbon, The sine-Gordon equation as a model classical field theory, *Nuovo Cimento B* 25 (1975) 497-512.
- [61] R. Miura, The Korteweg-de Vries equation: A survey of results, *SIAM Rev.* 18 (1976) 412-459.
- [62] H. Schamel, A modified Korteweg-de Vries equation for ion acoustic waves due to resonant electrons, *J. Plasma Phys.* 9 (1973) 377-387
- [63] C. Gu, H. Hu, Z. Zhou, *Darboux Transformations in Integrable Systems* (Springer, New York, 2005).